Geophysical Journal International

Geophys. J. Int. (2013) **192,** 573–585 doi: 10.1093/gji/ggs033

Derivation of 3-D coseismic surface displacement fields for the 2011 M_w 9.0 Tohoku-Oki earthquake from InSAR and GPS measurements

J. Hu,[1] Z. W. Li,[1] X. L. Ding,[2] J. J. Zhu[1] and Q. Sun[1]

[1]*School of Geosciences and Info-Physics, Central South University, Changsha, Hunan, P.R. China. E-mail: zwli@csu.edu.cn*
[2]*Department of Land Surveying and Geo-Informatics, Hong Kong Polytechnic University, Hung Hom, Kowloon, Hong Kong, P.R. China*

Accepted 2012 October 16. Received 2012 October 12; in original form 2012 May 3

SUMMARY

Interferometric synthetic aperture radar (InSAR) and global positioning system (GPS) have obvious deficiencies for monitoring surface deformations, for example, 1-D line-of-sight (LOS) measurements for InSAR and spatially very sparse observations for GPS. In this paper, InSAR and GPS measurements are integrated to derive spatially high-resolution 3-D coseismic surface displacement fields of the 2011 M_w 9.0 Tohoku-Oki, Japan earthquake. A unified simultaneous least squares (USLS) approach is developed to minimize the inconsistence between the InSAR results from adjacent paths. 3-D ground displacements are then derived by integrating the InSAR and the GPS measurements with the method of weighted least squares (WLS). Comparisons with independent GPS measurements show that the root mean square errors (RMSEs) of the derived 3-D displacements are 6.30, 4.57 and 1.29 cm for the vertical, east and north components, respectively. The 3-D coseismic displacement map shows that the Honshu Island moved eastwards towards the epicentre and subsided in the eastern part. The maximal displacements in the vertical, east and north directions are −1.5, 5.0 and −2.0 m, respectively. The effects of the density of GPS sites on the InSAR/GPS integration are also investigated. The experimental results reveal that lower to 70 km spatial resolution's GPS observations are adequate to guarantee the accuracies of the 3-D displacements for the Tohoku-Oki earthquake. This demonstrates the applicability of the developed WLS-based InSAR/GPS integration method, as in general the GPS observations are not as dense as those in this study area. Based on the spatially high-resolution 3-D surface displacement fields, we estimate the high-resolution and 3-D strain of the Tohoku-Oki earthquake. The preliminary results show that the Honshu Island suffers from an evident dilatation and shear during the seismic event.

Key words: Image processing; Spatial analysis; Satellite geodesy; Radar interferometry; Earthquake ground motions.

1 INTRODUCTION

Situated at the junction of the Pacific, Philippine, North American and Eurasian plates and in the circum-Pacific seismic belt, Japan has experienced frequent earthquakes. At 05:46:24 (UTC) of 2011 March 11, a destructive earthquake of M_w 9.0 occurred in the northeast coast of Honshu. The epicentre is offshore, 129 km east of the city of Sendai (Chu *et al.* 2011; Kato *et al.* 2012). It is reported that the earthquake and the tsunami triggered by the earthquake caused at least 15 000 deaths, 4000 missing, a large number of destroyed buildings and immeasurable impact on the environment due to the pollution from the leaked radioactive contaminants (Daniell & Vervaeck 2011).

After the Tohoku-Oki earthquake, GPS and InSAR observations have been used to investigate the coseismic displacement and the trigger mechanism of the seismic event. For example, a coseismic displacement field from the GPS Earth Observation Network (GEONET) was generated by the ARIA team from JPL and Caltech (available from ftp://sideshow.jpl.nasa.gov/pub/usrs/ARIA/). Spatially continuous displacement fields have also been produced from interferometric processing of SAR data by institutions such as the Japan Aerospace Exploration Agency (JAXA), Kyoto University, the Hong Kong Polytechnic University, Tohoku-Oki INGV Team, the Italian Space Agency (ASI), respectively (available from the Supersites http://supersites.earthobservations.org/).

However, these coseismic displacement fields have been constructed from InSAR or GPS data alone. Although they have shown that considerable ground movements around the Honshu Island occurred (e.g. Kobayashi *et al.* 2011; Feng *et al.* 2012), complete and spatially continuous 3-D surface displacement field associated with the earthquake is not yet available. The InSAR measurements are spatially

© The Authors 2012. Published by Oxford University Press on behalf of The Royal Astronomical Society.

GJI Gravity, geodesy and tides
Downloaded from http://gji.oxfordjournals.org/ at The Hong Kong Polytechnic University on February 11, 2015

continuous but are only sensitive to the surface displacement in the radar line-of-sight (LOS) direction (Wright *et al.* 2004). The GPS observations are 3-D but are available only at limited GPS stations. The spatial resolution of the GPS stations in the GEONET is about 25 km (Sagiya 2004).

It is well known that quantitative analysis of 3-D coseismic deformation is imperative in understanding the seismic ruptures and plate tectonics of an area (Fialko *et al.* 2001; Bos *et al.* 2004; Chlieh *et al.* 2004; Funning *et al.* 2005). The complementarities of InSAR and GPS measurements offer a great opportunity to infer 3-D displacements by appropriately integrating the measurements. Several approaches have recently been proposed to estimate 3-D displacement fields by integrating InSAR and GPS measurements. Gudmundsson *et al.* (2002) first merged the InSAR and GPS measurements to derive the 3-D surface displacement for the Iceland. In their study, the optimal solution was achieved by the Markov random field-based regularization and the simulated annealing algorithm. Subsequently, a revised method, termed analytical optimization (AOM), was developed by Samsonov *et al.* (2007) to map the 3-D displacement filed of Southern California from InSAR and GPS measurements. Although the time-consuming procedure of simulated annealing is avoided, the AOM is easily suffered from the numerical instability induced by the sparse and/or unevenly distributed GPS measurements. Guglielmino *et al.* (2011) proposed a SISTEM approach to obtain the 3-D displacement map of Mount Etna, in which the commonly required step of the GPS interpolation was exempted. However, the SISTEM may not be suitable to investigate large ground movements since it is developed based on the small deformation theory. Recently, Hu *et al.* (2012) introduced the variance component estimation (VCE) approach to weigh the InSAR and GPS measurements in the determination of 3-D surface displacements. This method does not require the *a priori* information on the stochastic model of the measurements but expects enough redundant measurements.

We will in this paper retrieve the 3-D coseismic surface displacement field of the 2011 Tohoku-Oki earthquake by appropriately integrating the InSAR and GPS measurements in the area. PALSAR ascending acquisitions from five adjacent satellite paths and ASAR descending acquisitions from three adjacent satellite paths are first assembled to determine the coseismic deformation of the area in the respective LOS directions. The derived coseismic deformations are calibrated with GPS data and the proposed unified simultaneous least squares (USLS) approach to minimize the discrepancies between adjacent satellite paths. 3-D displacement measurements from 295 GPS stations of the GEONET are also deployed to infer spatially continuous coseismic deformation maps by interpolating the GPS measurements to the lattice of the InSAR measurements. The method of weighted least squares (WLS) is then used to integrate the InSAR and GPS results to produce the 3-D coseismic deformation maps. We prefer the WLS approach rather than the methods of SISTEM and VCE because on one hand the coseismic displacements might be too tremendous to support the small deformation theory adopted by the SISTEM, and on the other the VCE method could not be carried out when the available data are very limited. In addition, the WLS approach is more straightforward and easy to implement than the afore-mentioned methods. The derived 3-D displacements are compared with the GPS measurements at 32 independent GPS stations (not included in the GPS/InSAR integration) to evaluate the quality of the results. In addition, we will conduct experiments to investigate the effects of the density of GPS sites on the InSAR/GPS integration for this area.

2 DATA PROCESSING AND ANALYSIS

The SAR data available for the study include L-band ALOS PALSAR images acquired from five ascending paths, 401–405, and C-band Envisat ASAR images from three descending paths, 74, 347 and 189. The areas of coverage of the SAR acquisitions are shown in Fig. 1. Table 1 provides further the basic parameters of the images.

The GEONET is one of the densest continuous GPS networks in the world. GPS observations at 327 GEONET sites are used in this study. The GPS data are processed and made public by the ARIA team from JPL and Caltech. 295 of the GPS stations will be used for estimaxxting the 3-D coseismic surface deformation, and 32 will be used to validate the derived 3-D displacement field. The locations of the GPS stations used for the estimation computation and for the validation are plotted as triangles and squares respectively in Fig. 1.

2.1 Estimation of LOS coseismic deformation of Tohoku-Oki earthquake from InSAR

For each satellite path listed in Table 1, the commonly used 2-pass InSAR data processing approach is applied to retrieve the surface displacement. The raw images of the same path are concatenated to produce a long strip single look complex (SLC) image with the GAMMA software. A SAR focusing problem is encountered in processing the ASAR images of path 189, causing a disconnection in the strip. The 3 arcsec SRTM data of the study area is used to simulate and eliminate the topographic component from the interferograms. The shaded relief map of the SRTM data are depicted in Fig. 1. For the descending Envisat ASAR acquisitions, the DORIS data provided by ESA is exploited to refine the orbit state vectors. While for the ascending ALOS PALSAR acquisitions, only the range and range rate (RARR) orbit information, that is, rapid orbit information, is adopted in the processing. Multilook operations with 15 and 20 pixels for PALSAR data and 15 and 3 pixels for ASAR data, respectively in the azimuth and the range directions, respectively are carried out to reduce the computation burden and the noise in the phase data, which yields interferograms with a final resolution of about 60 m $\times$ 60 m. Before unwrapping the interferograms with the minimum cost flow (MCF) algorithm (Costantini 1998), least squares based filtering is applied to further suppress the phase noise (Li *et al.* 2008).

Downloaded from http://gji.oxfordjournals.org/ at The Hong Kong Polytechnic University on February 11, 2015

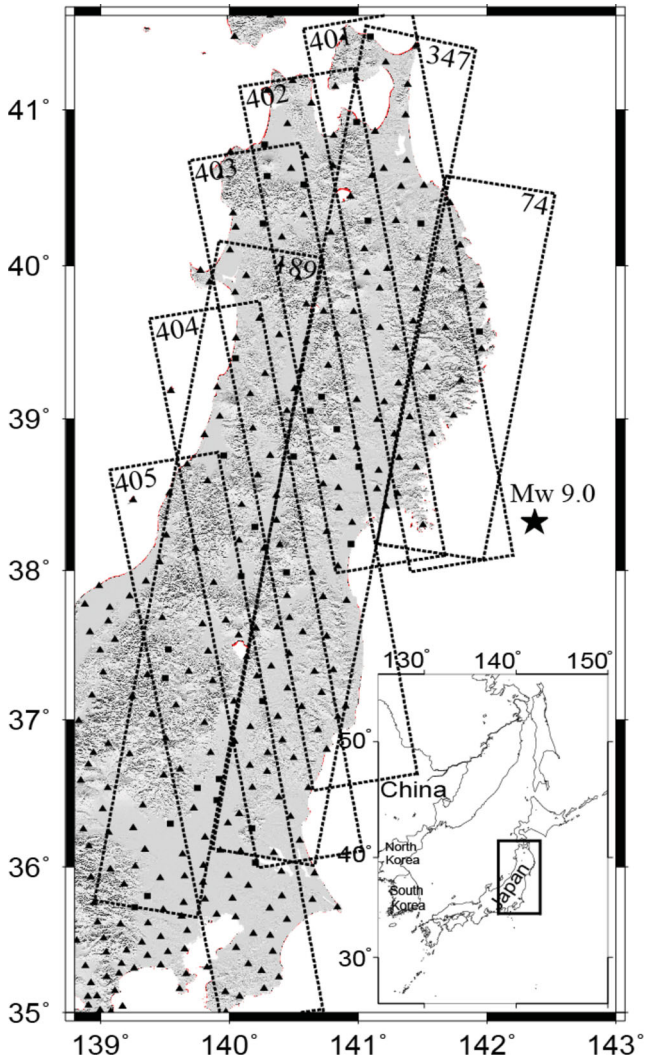

Figure 1. Shaded relief map of the Honshu Island. The rectangles in dotted lines indicate the frames of the PALSAR ascending and ASAR descending scenes. The locations of the GEONET GPS sites used for 3-D coseismic surface deformation estimation and for validation are shown as solid triangles and squares, respectively. The inset in the bottom right corner exhibits the location of the study area.

Table 1. Basic parameters of InSAR pairs used in the study.

Sensor	Pass	Path	Frames	Master	Slave	Temporal interval (d)	Perpendicular baseline (m)
PALSAR	A	401	760–800	2010 October 28	2011 March 15	138	1461
PALSAR	A	402	760–790	2010 September 29	2011 April 1	184	1229
PALSAR	A	403	730–780	2011 March 3	2011 April 18	46	358
PALSAR	A	404	720–760	2011 February 2	2011 March 20	46	832
PALSAR	A	405	700–740	2011 February 19	2011 April 6	46	402
ASAR	D	74	2763–2889	2011 March 2	2011 April 1	30	−134
ASAR	D	347	2763–2907	2011 February 19	2011 March 21	30	−171
ASAR	D	189	2763–2907	2011 March 10	2011 April 9	30	−323

Figs 2(a) and 3(a) show the coseismic surface displacements derived from the ascending PALSAR and the descending ASAR interferograms, respectively. The displacements from both the PALSAR and the ASAR data are rewrapped, where one fringe represents 11.8 cm surface displacement in the LOS directions in both sets of the results. Obvious discrepancies can be seen between the adjacent paths, particularly in the displacement map from the PALSAR data.

The errors are most likely induced by the process of removal of the flat-earth trend with inaccurate orbit state vectors (Feng *et al.* 2012). The deformations caused by the foreshocks, aftershocks, post-seismic deformation and possible ionospheric and tropospheric effects may also contribute to the errors (Feng *et al.* 2010; Grapenthin & Freymueller 2011; Ozawa *et al.* 2011). Such ramps are usually corrected within a single path by a bilinear or biquadratic model fitted with the differences between the GPS projected and InSAR measured LOS displacements. Then the corrected displacement fields are concatenated between adjacent paths (called single-path correction hereinafter) to form a complete

Downloaded from http://gji.oxfordjournals.org/ at The Hong Kong Polytechnic University on February 11, 2015

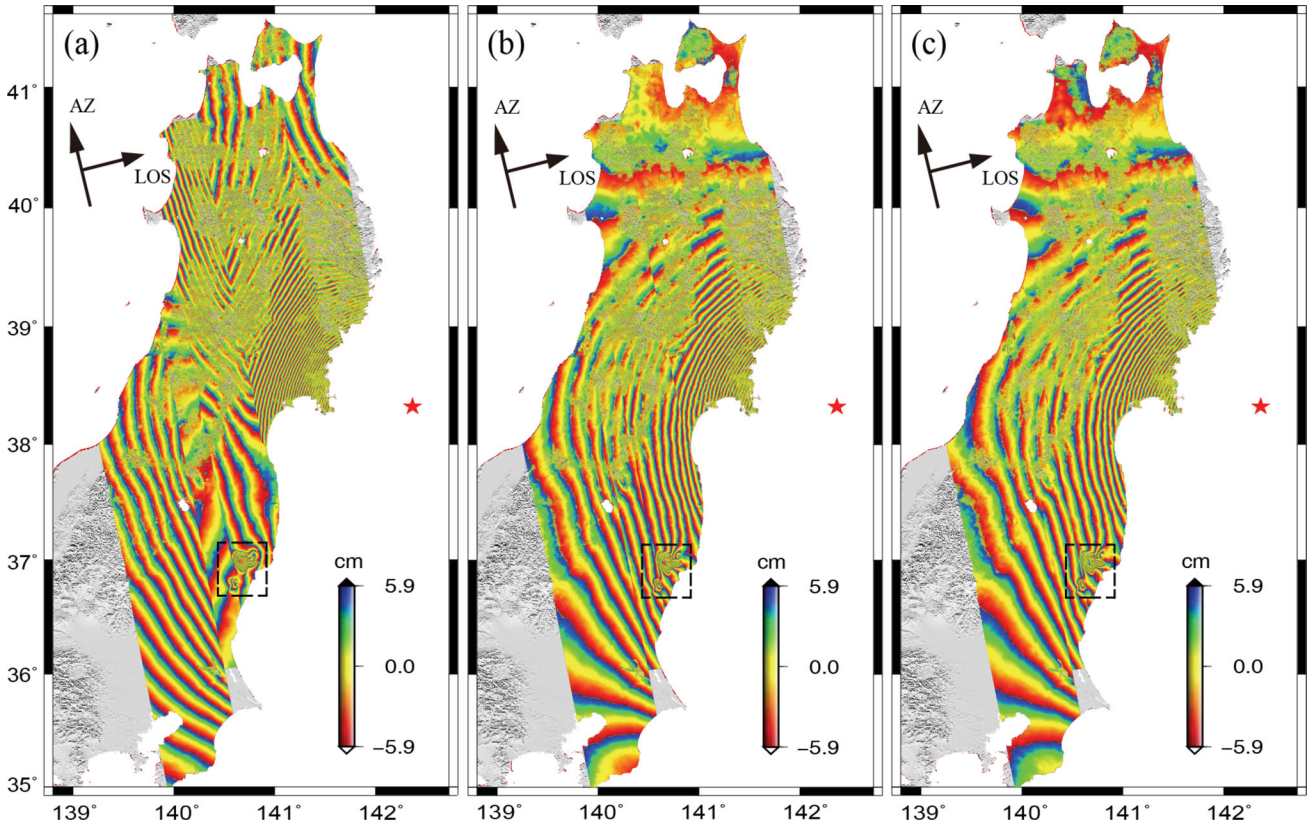

Figure 2. The coseismic displacements derived from the PALSAR ascending interferograms without correction (a), with single-path correction (b) and with multipath correction (c), respectively. AZ and LOS represent the azimuth and radar line-of-sight directions, respectively. Each colour cycle represents 11.8 cm surface deformation along the LOS direction. The dashed box shows the location of the two aftershocks occurred in 2011 March 19 and April 11.

displacement map (e.g. Kobayashi *et al.* 2011; Feng *et al.* 2012). However, the inconsistency between the adjacent paths is not considered in the single-path correction.

We propose in this study to use the USLS approach, which has been used by Liu *et al.* (2008) to remove glacier velocity discontinuities between adjacent image frames, to combine the InSAR results from the different paths and remove the discrepancies between them (called multipath correction hereinafter). The method will be applied to PALSAR and ASAR processing, respectively. The implementations are as follows:

(1) For InSAR results from adjacent paths i and $i+1$, we choose the GEONET GPS stations within the areas covered by the SAR scenes as control points (illustrated by triangles in Fig. 4), and a set of ground points within the overlapping area between the two paths as tiepoints (illustrated by dots in Fig. 4). Permanent scatterers in the images, for example, rocks and buildings, can often be identified and used as such tiepoints.

(2) For a control point in path i, assuming that I_i and G_i are its displacements derived from InSAR and GPS, respectively, a biquadratic model can be constructed based on the displacements of the controls points,

$$I_i - G_i = a_{i,0} + a_{i,1}x_i + a_{i,2}y_i + a_{i,3}x_iy_i + a_{i,4}x_i^2 + a_{i,5}y_i^2, \tag{1}$$

where x_i and y_i are coordinates of the point in path i; $a_{i,0} \ldots a_{i,5}$ are model parameters to be estimated for path i. Similarly, we can construct a model for any control point in path $i+1$

$$I_{i+1} - G_{i+1} = a_{i+1,0} + a_{i+1,1}x_{i+1} + a_{i+1,2}y_{i+1} + a_{i+1,3}x_{i+1}y_{i+1} + a_{i+1,4}x_{i+1}^2 + a_{i+1,5}y_{i+1}^2. \tag{2}$$

(3) For the tiepoints in the overlapping area between paths i and $i+1$, assume that T_i and T_{i+1} are the InSAR derived displacements from paths i and $i+1$, respectively. Similar to eqs (1) and (2), an equation for a tiepoint can be obtained

$$T_{i+1} - T_i = a_{i+1,0} + a_{i+1,1}x + a_{i+1,2}y + a_{i+1,3}xy + a_{i+1,4}x^2 + a_{i+1,5}y^2 - a_{i,0} - a_{i,1}x - a_{i,2}y - a_{i,3}xy - a_{i,4}x^2 - a_{i,5}y^2. \tag{3}$$

(4) Assuming m control points and n tiepoints are used, we can obtain a total of $m+n$ observation equations based on eqs (1)–(3), while the number of unknown parameters is 12. When $m+n \geq 12$, a WLS adjustment can be carried out to resolve the unknown parameters. The weights of the observations are determined according to the coherence of the InSAR images. An iterative procedure is implemented to exclude the points with large least squares residuals.

Downloaded from http://gji.oxfordjournals.org/ at The Hong Kong Polytechnic University on February 11, 2015

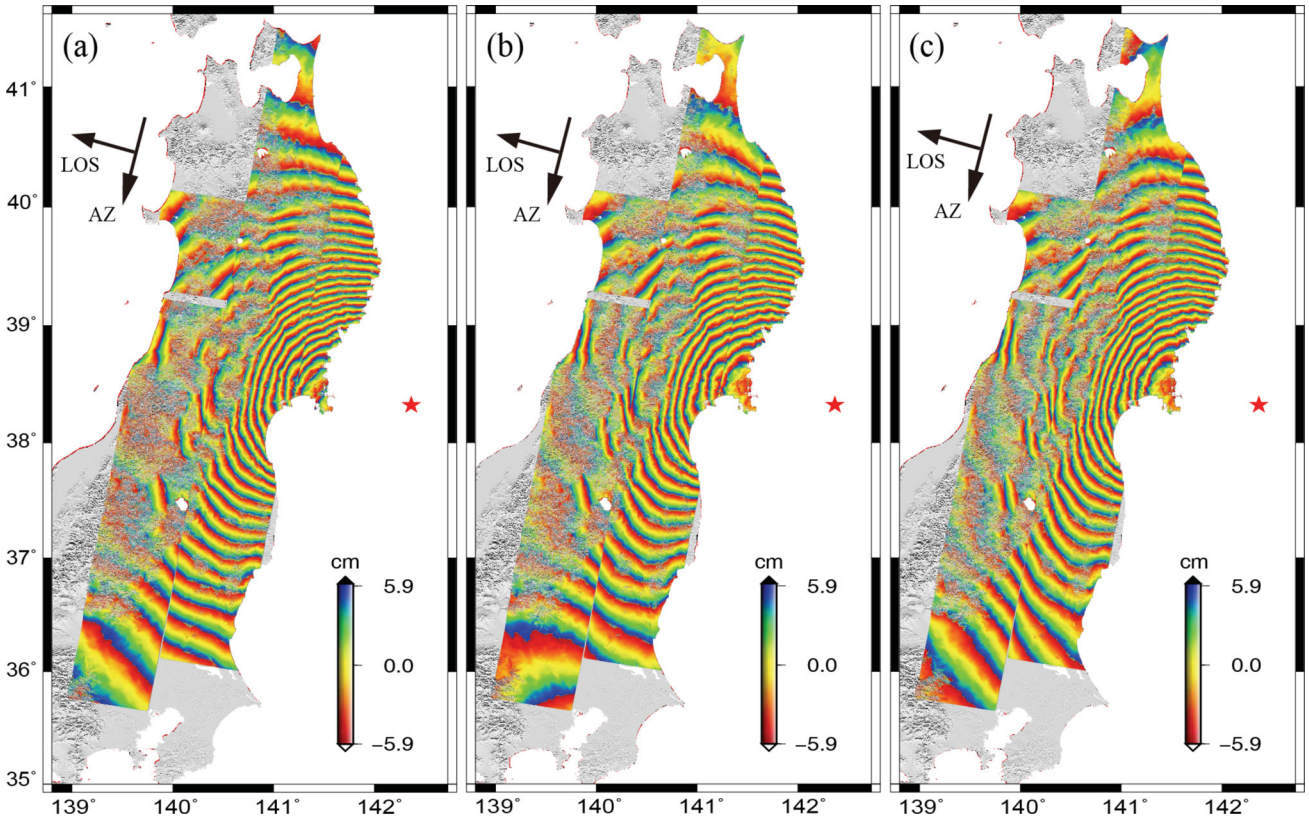

Figure 3. The coseismic displacements derived from the ASAR descending interferograms without correction (a), with single-path correction (b) and with multipath correction (c), respectively. AZ and LOS represent the azimuth and radar line-of-sight directions, respectively. Each colour cycle represents 11.8 cm surface deformation along the LOS direction.

(5) Finally, the ramps in paths i and $i + 1$ are computed based on the estimated parameters $a_{i,0} \ldots a_{i,5}$ and $a_{i+1,0} \ldots a_{i+1,5}$, respectively, and then removed from the InSAR results of paths i and $i + 1$ to produce the refined displacement results.

The above operations can be expanded to InSAR results from more than two adjacent paths. For example, in this study, they are applied to five paths for PALSAR data and three paths for ASAR data. The PALSAR LOS displacements after applying the traditional single- and the proposed multipath corrections respectively are shown in Figs 2(b) and (c). Note that all the LOS displacement results have been resampled into a regular grid of 9900 × 5400 pixels, with a pixel size of about 74 m × 74 m. It is clear from the results that both results are much better (e.g. more logical and less discrepancies between paths) than the original results. In addition, the results from multipath correction are superior to those from single-path correction. Figs 3(b) and (c) show the corresponding results from ASAR data after applying the single- and multipath corrections. As the orbit state vectors of ASAR data are more accurate, the corrections to the results are not as great as those to the PALSAR results. However, the consistency between the results from the different paths has also been improved by the multipath correction, although the performance of the correction is not as good as in the case of the PALSAR results due to the much smaller overlapping areas between the adjacent ASAR paths (see Fig. 1).

2.2 Coseismic deformation of Tohoku-oki Earthquake from GPS observations

The GPS measured coseismic surface displacement of the Tohoku-Oki earthquake is shown in Fig. 5. The arrows represent the deformation vectors at the GPS sites determined based on 5 min dynamic solutions, more specifically, the coordinate differences at the stations between the solutions at 5:40 and 5:55 UTC. It is evident that the ground movements are very significant in both the vertical and the horizontal directions. As shown in Fig. 5(a), the east–southeastern part of the Honshu Island experienced significant subsidence, with the maximum reaching about 1.1 m at GPS site 0550 on the Oshika peninsula, while the west–northwestern part of the Honshu Island only went upwards slightly. Fig. 5(b) gives the horizontal coseismic displacements at the GPS sites that were all towards the focal region with the largest displacement exceeding 5 m also at GPS site 0550.

Although the spatial resolution of the GEONET reaches about 25 km, it cannot reveal surface deformation signatures with wavelength shorter than that. This motivates us to investigate an integration of GPS and InSAR measurements. In doing this, the GPS displacement measurements at the 295 sites are interpolated into the same pixel lattice of the geocoded InSAR maps. The Ordinary Kriging (OK) technique with a linear variogram model is used in the interpolation (Samsonov *et al.* 2007). Considering that the vertical GPS measurements are lower

Downloaded from http://gji.oxfordjournals.org/ at The Hong Kong Polytechnic University on February 11, 2015

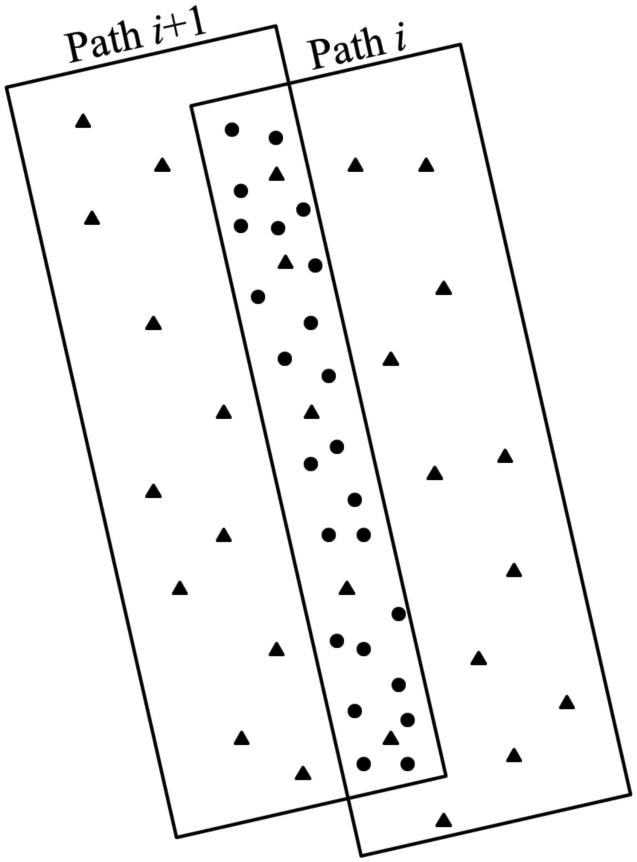

Figure 4. Sketch map of multipath correction by USLS. Solid triangles and circles represent the control points and tiepoints, respectively.

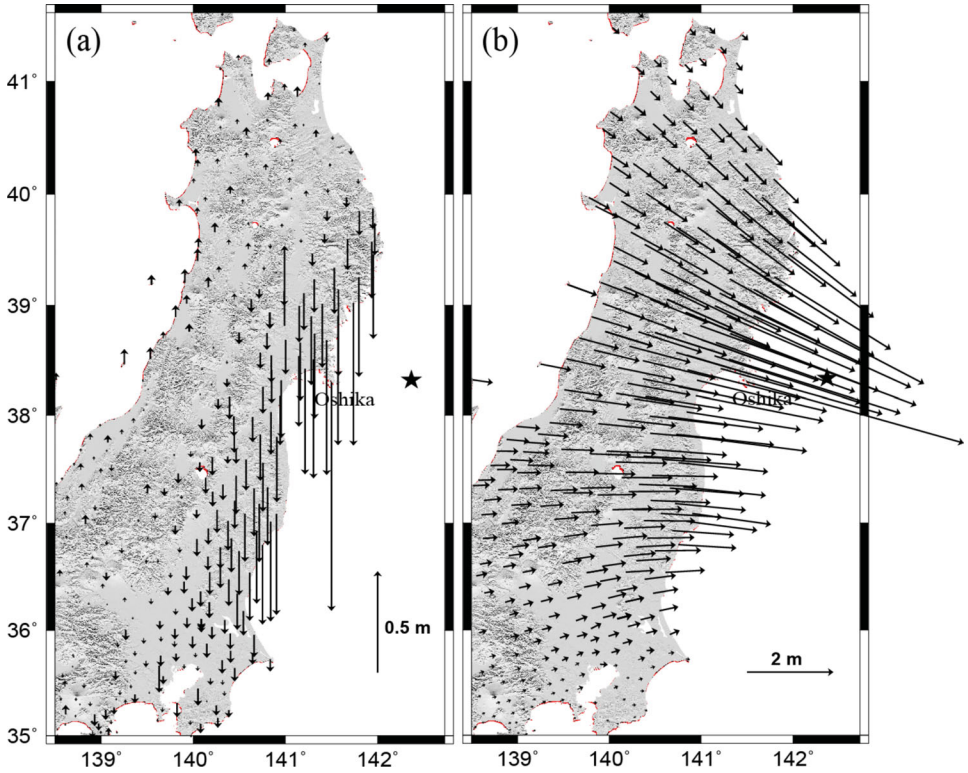

Figure 5. The GPS measured coseismic surface displacement of the Tohoku-Oki earthquake in vertical (a) and horizontal (b) directions, respectively.

Downloaded from http://gji.oxfordjournals.org/ at The Hong Kong Polytechnic University on February 11, 2015

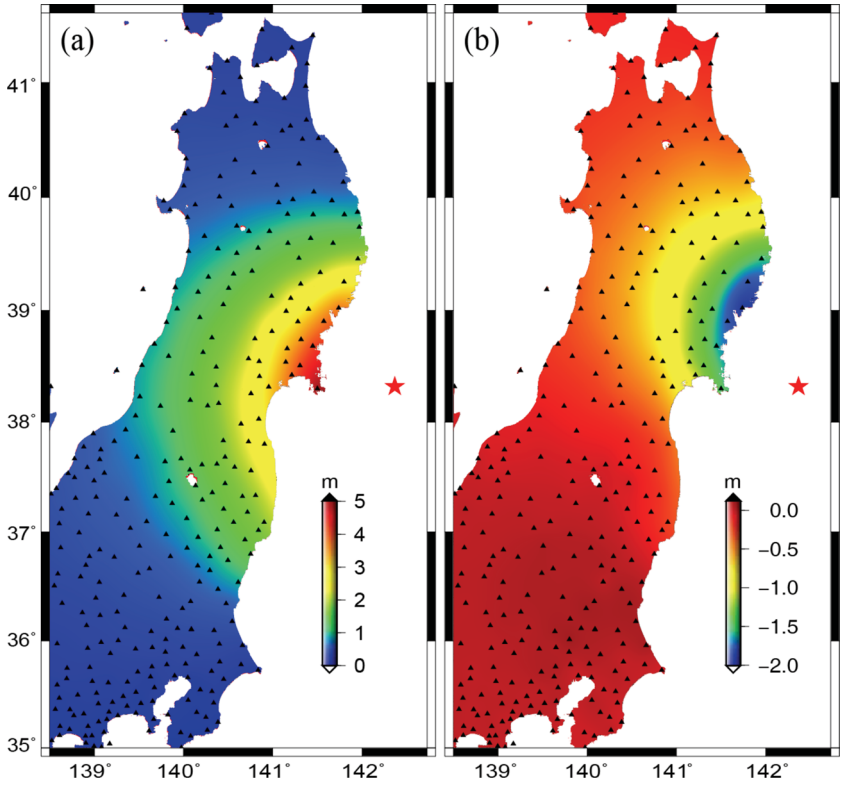

Figure 6. The interpolated GPS displacement maps of the Tohoku-Oki earthquake in east–west (a) and north–south (b) directions, respectively. Solid triangles show the locations of the GEONET GPS sites used for interpolation.

in accuracy than the horizontal ones (Gudmundsson *et al.* 2002) and have limited contribution to the InSAR/GPS integration (Hu *et al.* 2012), they are not included in the 3-D coseismic displacement computation.

Figs 6(a) and (b) show the interpolated GPS displacement maps in the east–west and north–south directions, respectively. It is observed that both of the coseismic displacement maps are very smooth and increase gradually from the far field towards the focal region, which are typical forms of ground movement caused by seismic shock.

2.3 Determination of 3-D coseismic displacement of Tohoku-Oki earthquake

To resolve the 3-D coseismic displacement field of the Tohoku-Oki earthquake, a WLS approach is applied to combine the four displacement vectors obtained in the above analysis, that is, the two InSAR LOS measurements $D_{\text{los}}^{\text{palsar}}$ and $D_{\text{los}}^{\text{asar}}$ and the two interpolated GPS horizontal measurements (with the same lattice as InSAR) $D_{\text{east}}^{\text{gps}}$ and $D_{\text{north}}^{\text{gps}}$. The problem is formulated for each pixel as

$$L = B \cdot u, \tag{4}$$

where $L = [\, D_{\text{los}}^{\text{palsar}} \;\; D_{\text{los}}^{\text{asar}} \;\; D_{\text{east}}^{\text{gps}} \;\; D_{\text{north}}^{\text{gps}} \,]^{\text{T}}$ denotes the measurement vector; $u = [\, u_{\text{vertical}} \;\; u_{\text{east}} \;\; u_{\text{north}} \,]^{\text{T}}$ contains the unknown displacements in the vertical, east and north directions, respectively; and B is the design matrix,

$$B = \begin{bmatrix} \cos(\theta_{asar}) & -\sin\left(\alpha_{asar} - \frac{3\pi}{2}\right)\sin(\theta_{\text{asar}}) & -\cos\left(\alpha_{\text{asar}} - \frac{3\pi}{2}\right)\sin(\theta_{\text{asar}}) \\ \cos(\theta_{palsar}) & -\sin\left(\alpha_{\text{palsar}} - \frac{3\pi}{2}\right)\sin(\theta_{\text{palsar}}) & -\cos\left(\alpha_{\text{palsar}} - \frac{3\pi}{2}\right)\sin(\theta_{\text{palsar}}) \\ 0 & 1 & 0 \\ 0 & 0 & 1 \end{bmatrix},$$

where θ and α represent the incidence and azimuth angles, respectively.

The WLS solution of the 3-D displacements is obtained by

$$u = (B^T \Sigma_L^{-1} B)^{-1} \cdot B^T \Sigma_L^{-1} L, \tag{5}$$

where Σ_L is the variance–covariance matrix of the measurements. Similar to the previous studies (e.g. Samsonov *et al.* 2007; Hu *et al.* 2010), for the sake of simplicity, the correlation between the measurements is not considered so that Σ_L is a diagonal matrix. In order to determine the weight of each InSAR measurement, the standard deviation of an InSAR measurement is estimated on a pixel by pixel basis by using a 5×5 moving window in the displacement maps. The calculated standard deviations of the GPS measurements need however to be scaled

Downloaded from http://gji.oxfordjournals.org/ at The Hong Kong Polytechnic University on February 11, 2015

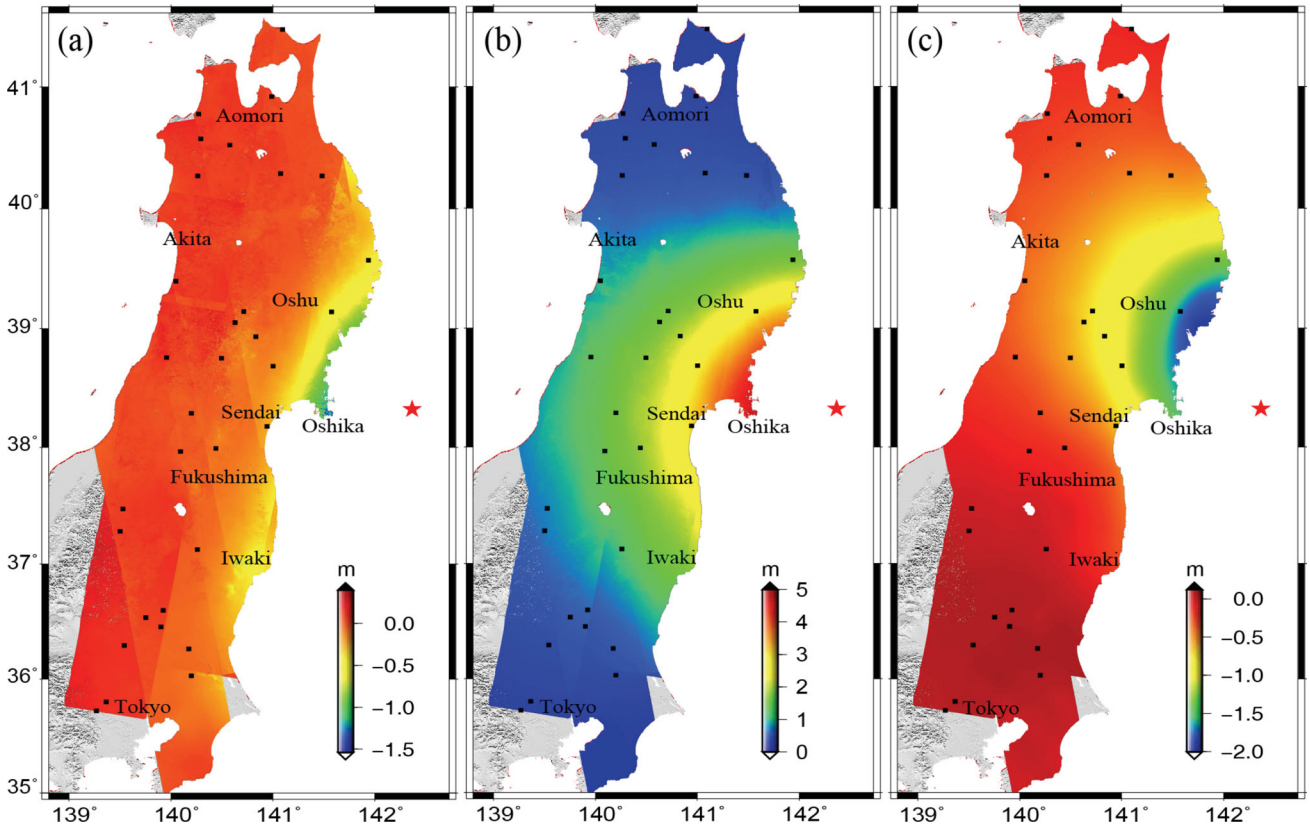

Figure 7. The 3-D coseismic surface displacements of the Tohoku-Oki earthquake obtained from InSAR and GPS integration. (a) Vertical component, (b) east–west component and (c) north–south component. Solid squares show the locations of the GEONET GPS sites used for validation.

according to the uncertainties created by the OK interpolation (Samsonov *et al.* 2007). To further reduce the high-frequency noise, the derived 3-D displacements are smoothed with a 5 × 5 mean filter.

Although the GPS observations are used twice in the 3-D displacements derivation, that is, the multipath correction and the WLS integration of GPS and InSAR, it does not tend to bias the final solution. The reason is that in the multipath correction the sparse GPS observations are mainly used to remove the long-wavelength InSAR signals (i.e. orbital ramps) by least squares algorithm, and the achieved InSAR displacements are generally with moderate- to short-wavelength and will not correlate with the sparse GPS observations strongly. This can help to stabilize the WLS system in eq. (4) from highly correlated measurements and rank deficiency, and thus will not bias the final 3-D displacement solution very much.

Fig. 7 presents the 3-D coseismic surface displacements obtained. It should be noted that the WLS computation has also been performed for the pixels that have only one InSAR LOS measurement, either from PALSAR or from ASAR. It is observed from the derived 3-D solution that the vertical displacements range from −1.54 to 0.40 m, while the east–west and north–south displacements vary from 0.04 to 5.00 m and from −2.00 to 0.13 m, respectively. A comparison between the solution and the GPS observations at the 32 validation stations is carried out to evaluate the quality of the results. The validation GPS stations (the squares in Fig. 7) were not included in the InSAR and GPS integration so that they are independent to the 3-D solution. As seen from the results in Figs 8(a)–(c), very good agreements are found in all the three deformation components. Statistical results show that the root mean square errors (RMSEs) are 6.30, 4.57 and 1.29 cm for the vertical, east and north components, respectively, while the corresponding mean errors are 1.99, 2.05 and 0.02 cm.

3 DISCUSSION

The accuracy of the derived 3-D surface displacements depends on the accuracy of the InSAR and GPS measurements. It is complicated to assess the errors of the InSAR measurements in this study as interferograms from different sensors and paths and with different spatial-temporal baselines are involved in the computation. Besides, owing to the differences of the SAR acquisition dates between adjacent paths (about half a month), errors can be introduced to the InSAR measurements too due to the post-seismic deformation that has proceeded with tens of centimetres (Ozawa *et al.* 2011). However, the effect of the post-seismic deformation has been greatly minimized together with the orbit ramps by the USLS approach. This reason is twofold. First, the GPS observations, which are used as the control points in the USLS approach, is completely coseismic deformation measurements because they are just ∼6 min before and ∼9 min after the event. Second, the post-seismic deformations behave as regular and gradually varied fringes, especially for the dominant horizontal component (Ozawa *et al.* 2011), which generally share similar signatures with the orbit ramps in space. Note that the effects of aftershocks cannot be corrected by

Downloaded from http://gji.oxfordjournals.org/ at The Hong Kong Polytechnic University on February 11, 2015

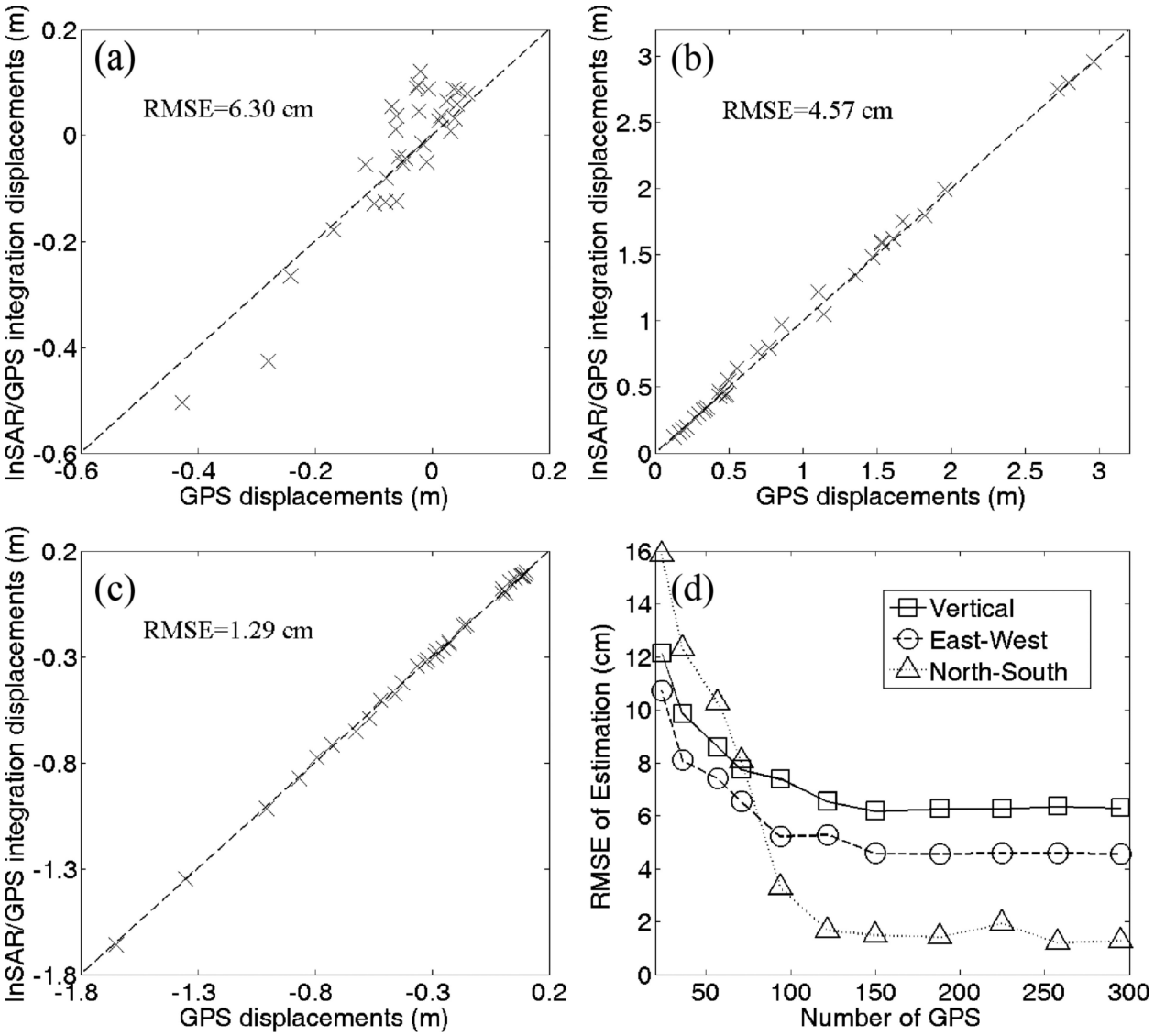

Figure 8. Comparisons of the 3-D coesismic displacements of the Tohoku-Oki earthquake derived from InSAR/GPS integration and GPS observations alone at the 32 validation stations. (a) Vertical component, (b) east–west component and (c) north–south component. (d) Averaged RMSEs of the 3-D displacement estimations versus the number of GEONET GPS sites used for the estimations.

the USLS approach. In particular, two local deformations caused by the 2011 March 19 and April 11 aftershocks are distinguished in the coseismic displacements derived from the PALSAR ascending interferograms with multipath correction (see the dashed box in Fig. 2). In unweighted InSAR and GPS integration, this aftershock effect will be introduced into the 3-D displacement solution. However, we find that in our WLS solution the standard deviations of the aftershock deformations from the PALSAR ascending measurements are quite larger than those from the ASAR descending measurements and the interpolated GPS measurements [see the dashed box in Fig. S2(a)]. The weight of the aftershock deformations will thus be degraded in the WLS adjustment. This can help to diminish the effect of the aftershock in the final 3-D displacement derivation.

For the L-band PALSAR data, the results in the mountainous areas are noisier, especially for paths 401 and 402 that have relatively larger spatial and temporal baselines (see Figs 2a–c). The ionospheric disturbances in the PALSAR data are believed to be small in this study, as the azimuth streaks are not prominent in the azimuth displacement field derived from the offset-tracking method (see Fig. S1). The C-band ASAR results from path 189 are affected more by the spatial decorrelation than those from paths 74 and 347 (see Figs 3a–c). For the great earthquake with magnitude 9.0, the tropospheric effects, which are highly correlated with elevation and typical on level of several centimetres (Li *et al.* 2012), are believed to be insignificant in the PALSAR and ASAR results. The estimated standard deviations of the PALSAR and ASAR measurements are similar in areas with high coherence. While in other areas the qualities of the PALSAR and ASAR results are somewhat complementary. The GPS positioning accuracy is about 3 cm, with the standard deviation of the horizontal and vertical components being about 0.9 and 2.7 cm, respectively (Shao *et al.* 2011). It should be mentioned that InSAR and GPS observations covers inconsistent time interval, which degrades the accuracies of the 3-D displacement estimations further. As the LOS unit vectors in the vertical, east–west and north–south directions are about [0.89, −0.62, −0.11] and [0.91, 0.64, −0.11], respectively for the PALSAR ascending and ASAR

Downloaded from http://gji.oxfordjournals.org/ at The Hong Kong Polytechnic University on February 11, 2015

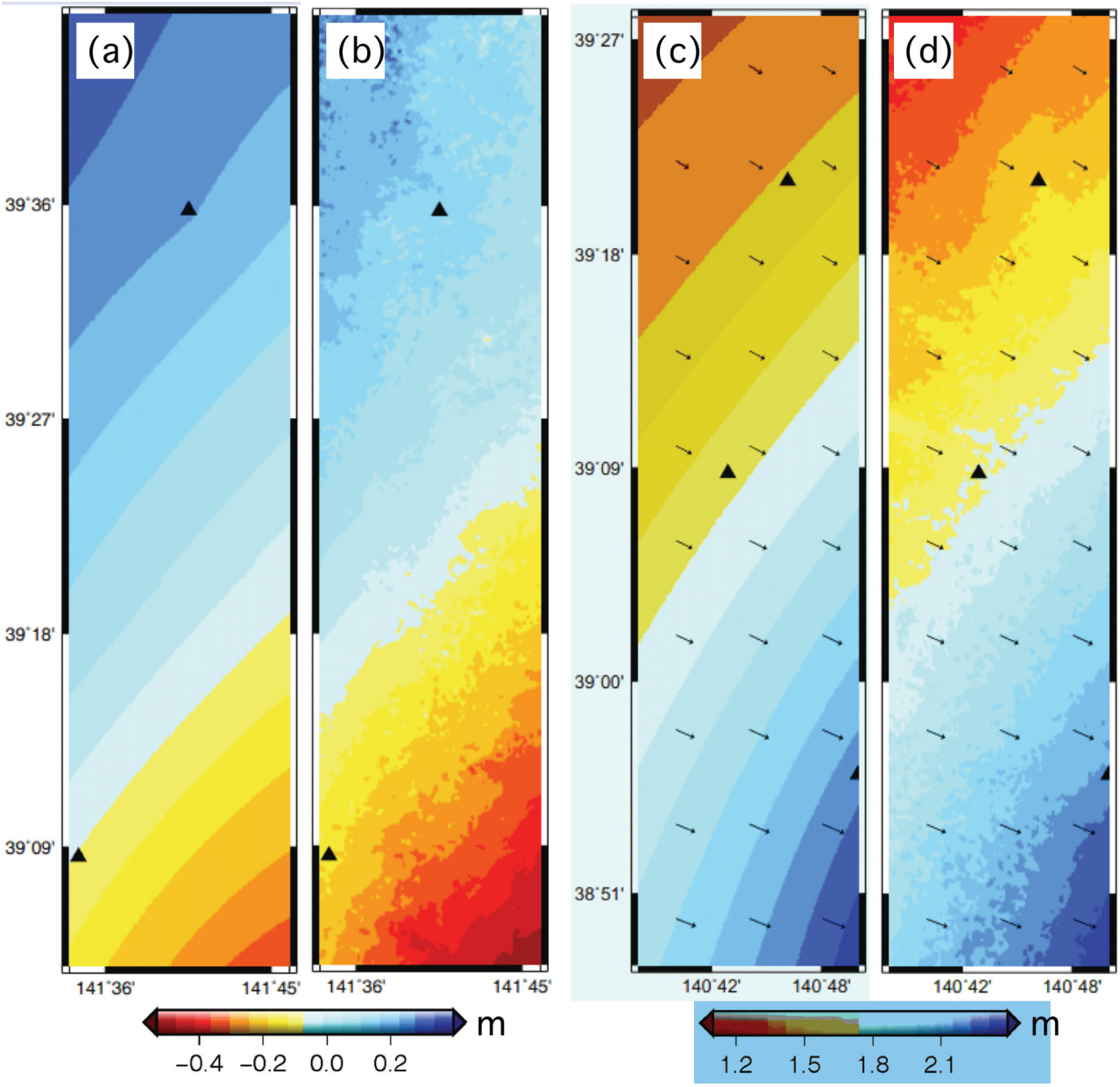

Figure 9. (a and b) The vertical displacement maps near the Oshu area derived from GPS interpolation and InSAR/GPS integration, respectively. (c and d) The horizontal displacement maps near the Akita area derived from GPS interpolation and InSAR/GPS integration, respectively. The colours and arrows represent the amplitude and direction of the horizontal displacements, respectively.

descending measurements, the InSAR observations are most sensitive to the vertical displacement, followed by the east–west displacement. Therefore, in the 3-D displacement inversion, the vertical components are influenced most by the InSAR results, while the north–south ones benefit mostly from the OK interpolation of GPS observations rather than the InSAR measurements. Therefore, the north–south components are sensitive to the errors induced by the OK interpolation. This could explain why the InSAR and GPS integrated solution fits the GPS results best in the north–south direction. It can also be demonstrated by the *SD* maps of the PALSAR, ASAR, GPS measurements and the derived 3-D displacement fields (see Figs S2 and S3), where the GPS north–south and InSAR LOS measurements' *SD*s mimic those of the north and vertical components of the 3-D displacements, respectively.

Nevertheless, the derived 3-D displacement field maintains a relatively high accuracy, that is, 6.30, 4.57 and 1.29 cm for the vertical, east and north components, respectively, as evaluated by the 32 independent GPS stations. This displacement field is essential for studying the 2011 Tohoku-Oki event, as its spatial resolution has been refined to about 70 m from 25 km configured by GPS observations alone. This is crucial to more exactly measure small- to moderate-sized ground deformation that cannot be captured by the sparse GPS data (although it is already the densest one in the world). For example, in the areas near Oshu and Akita, more detailed surface deformations (with resolutions of about 150 and 120 m for the vertical and horizontal components respectively as estimated by the method of modulation transfer function (Xiong *et al.* 2000), which are not observed in the interpolated GPS displacements, are existed in the derived 3-D displacement field

Downloaded from http://gji.oxfordjournals.org/ at The Hong Kong Polytechnic University on February 11, 2015

(as shown in Fig. 9). It is observed in Fig. 9 that there are only two GPS stations established in the about 20 km × 70 km area. The GPS interpolated displacements are extraordinarily regular and smooth, while the InSAR/GPS derived 3-D displacements are with more variations and fractal-like features. It is well understood that the detailed and small-scale surface displacements could be affected by the disturbance of the ground surface, especially in regions where the terrain is precipitous. As the topography is generally characterized by the fractal-like features, so do the detailed and small scale coseismic displacements. This indicates that the InSAR/GPS derived 3-D displacements are more reasonable and authentic. We use two quantitative criteria, that is, correlation and information entropies, to evaluate the information content of the GPS interpolated and InSAR/GPS derived 3-D displacements. The results show that the correlation between the InSAR/GPS derived 3-D displacements and the GPS measurements at the 32 validation stations increases to 0.92 from 0.87 between the interpolated and the original GPS measurements at those stations. While the information entropies of the InSAR/GPS derived and the GPS interpolated 3-D displacements are 7.62 and 7.59 bits for vertical component, and 7.82 and 6.64 bits for horizontal component, respectively. Thus, an average improvement of about 9.1 per cent has been achieved, indicating that more information contents have been provided by the InSAR/GPS derived displacement field.

The accurate high-resolution 3-D coseismic surface deformation field derived from the InSAR/GPS integration (Fig. 7) also reveals well the ground displacements. Both the vertical and horizontal surface displacements increase and converge from West to East, with respect to the Japan Trench subduction zone. It is seen that the maximal ground motions occurred in the Oshika peninsula near the epicenter. The largest ground subsidence reached about 1.5 m, obviously larger than that determined from the GPS observations alone. The cities of Oshu and Sendai experienced about 2.8 m horizontal ground movements towards the focal region and about 0.3–0.2 m subsidence. The ground motions decreased significantly in the Akita and Aomori areas, the northeastern part of the Honshu Island. The Fukushima area experienced about −0.1, 1.8 and −0.2 m displacements in the vertical, east and north directions, respectively. Although the tsunami triggered by the earthquake is the predominant cause, the great ground movements in this area are also expected to contribute to the destruction of the Fukushima I and II Nuclear Power Plants, located about 34 km north of the Iwaki city. Being about 374 km away from the epicenter, Tokyo city also experienced 0.17 and 0.06 m displacements in the east and north directions, respectively, while only a very mild uplift, that is, 0.03 m, is detected in the area. The 3-D deformation field confirms that the Tohohu-Oki earthquake is most likely induced by a thrust of the Japan Trench (Hashimoto *et al.* 2009; Shao *et al.* 2011). However, near-field displacement on the seafloor cannot be depicted by the InSAR and GEONET GPS measurements, and that needs further investigation (Sato *et al.* 2011; Hashimoto *et al.* 2012).

To evaluate the applicability of the developed InSAR/GPS integration method when the GPS networks are not as dense as that of GEONET, we carried out a series of experiments by gradually reducing the number of GPS sites and doing the InSAR and GPS integration. As shown in Fig. 8(d), the averaged RMSEs of the 3-D displacement estimations all increase with the decrease of the number of GPS sites. However, the RMSEs only increase significantly when the involved GPS stations are less than about 100. Therefore, approximate 70 km for the spatial resolution of the GPS sites is adequate to guarantee the high accuracies of the 3-D displacements, at least for the Tohoku-Oki earthquake.

The spatially continuous 3-D coseismic surface deformation field also provides us an opportunity to investigate the strain of the Tohoku-Oki earthquake, with the characteristics of high spatial resolution and three-dimensionality. In this paper, we estimated three strain invariants, that is, dilatation, differential rotation magnitude and maximum shear strain (Vanicek *et al.* 2008), for each pixel in the derived 3-D displacement field by using a modified WLS inversion (Amighpey *et al.* 2009; Guglielmino *et al.* 2011). As shown in Fig. 10(a), the dilatation invariant field ranges from -3.5×10^{-4} to 1.7×10^{-4}. The expansion is dominant in most of the Honshu Island, especially in the northern part, which is mainly ascribed to the great ground movements toward the focal region. However, it is observed that the centre of the Honshu Island near the Sendai and Oshika areas are subject to large contractions. This is expected since the ground movements behave with a convergent trend from the upper and lower areas to the centre (Caporali *et al.* 2003). In the differential rotation magnitude invariant field (Fig. 10b), only up to 1.2×10^{-5} differential rotation are detected in the central part of the Honshu Island. Fig. 10(c) exhibits the maximum shear strain invariant field, which is similar to the distribution of the differential rotation magnitude invariant but reaches 7.0×10^{-3} for extreme condition. The location of the differential rotation magnitude and maximum shear strain conforms to the great contractions in the centre of the Honshu Island. The concentration of the three strain invariants can be used as a useful indication of blind faults (Amighpey *et al.* 2009). Although more work is needed to refine the strain analysis results, it is revealed by the derived strain invariants that the Honshu Island suffered from an evident dilatation and shear during the seismic event.

4 CONCLUSIONS

The 2011 M_w 9.0 Tohoku-Oki earthquake, one of the strongest earthquakes in recorded instrumental history, caused significant ground motion. We have presented a full 3-D coseismic surface displacement field of the earthquake derived from a WLS based integration of the available InSAR and GPS measurements. In order to fully cover the seismic event, the PALSAR images acquired on five ascending paths and ASAR images on three descending paths are employed. We develop a multipath correction (i.e. USLS) approach to better suppress the inconsistencies that emerge in the InSAR results of adjacent paths. The 3-D displacement results reveal clearly that the ground of the Honshu Island moved up to −1.5, 5 and −2 m, respectively in the vertical, east and north directions during the earthquake. Small- to moderate-sized coseismic displacements, which cannot be captured by the GEONET GPS measurements, are detected by the InSAR/GPS integration at the spatial resolution of about 70 m. The results provide useful insights into the spatial variation of the ground motion and the focal mechanism of the earthquake. The RMSEs between the InSAR/GPS integration and independent GPS measurements are 6.30, 4.57 and 1.29 cm in the

Downloaded from http://gji.oxfordjournals.org/ at The Hong Kong Polytechnic University on February 11, 2015

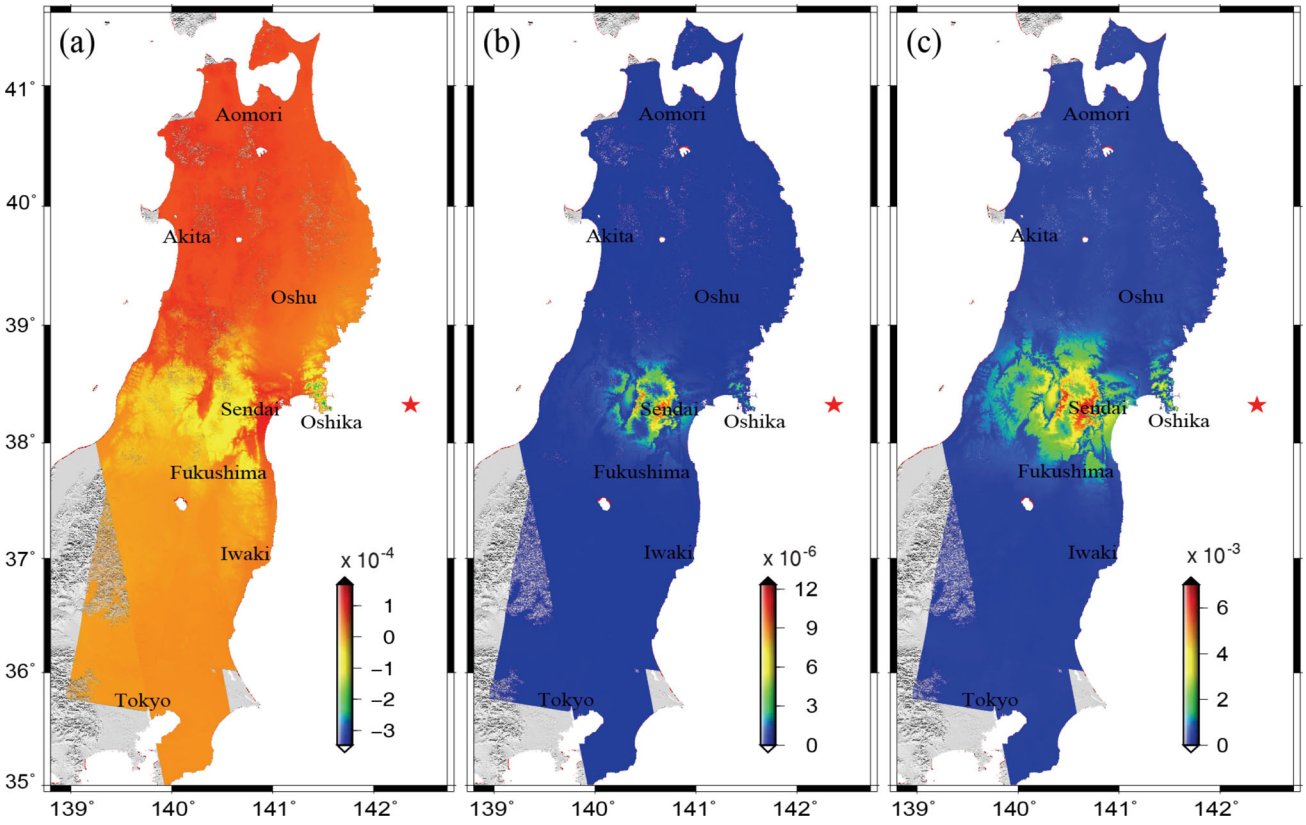

Figure 10. The strain invariants of the Tohoku-Oki earthquake obtained from the spatially continuous 3-D coseismic surface displacements. (a) Dilatation, (b) differential rotation magnitude and (c) maximum shear strain. All the three vectors are dimensionless.

vertical, east and north directions, respectively. The accuracies would no significantly degrade until the number of deployed GPS stations is less than about 100 for this area, which indicates a spatial resolution of approximate 70 km for GPS observations is tolerable for accurately estimating the 3-D displacements caused by the Tohoku-Oki earthquake. In addition, the spatially continuous strains are retrieved from the 3-D coseismic surface deformation field to exhibit the dilatation, rotation and shear due to the Tohoku-Oki earthquake.

Some limitations remain in this study. First, although the developed USLS approach can correct the orbital errors very well, the contribution from large aftershocks occurred during the investigated time period cannot be completely isolated from the interferometric phases. This would help to overestimate the final 3-D displacement field. Second, the determination of *a priori* variances of the InSAR and GPS measurements is vital in the integration of InSAR and GPS with the WLS adjustment. A simple empirical method is applied in this study, but could be improved by more robust algorithms, for example, VCE, when more independent observables are available (Hu *et al.* 2012). Third, although the derived strain invariants reveal considerable amount of the dilatation and shear associated with the Tohoku-Oki earthquake, the correlation between the strains and the faults should be further investigated.

ACKNOWLEDGMENTS

We thank the two anonymous reviewers for their constructive comments. The ALOS PALSAR data were provided by the Japanese Space Agency (JAXA). The ENVISAT ASAR data were from the GEO Geohazards Supersite. Preliminary GPS time series provided by the ARIA team at JPL and Caltech. All original GEONET RINEX data provided to Caltech by the Geospatial Information Authority (GSI) of Japan. Drs. Guangcai Feng and Lei Zhang assisted in assembling data. Several figures were plotted with the GMT software (Wessel & Smith 1998). The research was supported by the National Natural Science Foundation of China (Nos. 40974006 and 41222027), National High Technology Research and Development Program of China (No. 2012AA121301), National Key Basic Research and Development Program of China (No. 2012CB719903), the Research Grants Council of the Hong Kong Special Administrative Region (Project No.: PolyU 5154/10E), and the Scholarship Award for Excellent Doctoral Student from the Ministry of Education of China (No. 085201001).

REFERENCES

Amighpey, M., Vosooghi, B. & Dehghani, M., 2009. Earth surface deformation analysis of 2005 Qeshm earthquake based on three-dimensional displacement field derived from radar imagery measurements, *Int. J. appl. Earth Obs.,* **11,** 156–166.

Bos, A.G., Usai, S. & Spakman, W., 2004. A joint analysis of GPS motions and InSAR to infer the coseismic surface deformation of the Izmit, Turkey earthquake, *Geophys. J. Int.,* **158,** 849–863.

Caporali, A., Martin, S. & Massironi, M., 2003. Average strain rate in the Italian crust inferred from a permanent GPS network—II. Strain rate versus seismicity and structural geology, *Geophys. J. Int.,* **155,** 254–268.

Downloaded from http://gji.oxfordjournals.org/ at The Hong Kong Polytechnic University on February 11, 2015

Chlieh, M., De Chabalier, J.B., Ruegg, J.C., Armijo, R., Dmowska, R., Campos, J. & Feigl, K.L., 2004. Crustal deformation and fault slip during the seismic cycle in the North Chile subduction zone, from GPS and InSAR observations, *Geophys. J. Int.,* **158,** 695–711.

Chu, R.S., Wei, S.J., Helmberger, D.V., Zhan, Z.W., Zhu, L.P. & Kanamori, H., 2011. Initiation of the great Mw 9.0 Tohoku-Oki earthquake, *Earth planet. Sci. Lett.* **308,** 277–283.

Costantini, M., 1998. A novel phase unwrapping method based on network programming, *IEEE Trans. Geosci. Remote Sens.,* **36**(3), 813–821.

Daniell, J.E. & Vervaeck, A., 2011. The 2011 Tohoku Earthquake–CATDAT Situation Reports 1–26, Earthquake-Report.com.

Feng, G.C., Ding, X.L., Li, Z.W., Jiang, M., Zhang, L. & Omura, M., 2012. Calibration of InSAR-derived coseimic deformation map associated with 2011 Mw 9.0 Tohoku-Oki earthquake, *IEEE Geosci. Remote Sens. Lett.,* **9**(2), 302–306.

Feng, G.C., Hetland, E.A., Ding, X.L., Li, Z.W. & Zhang, L., 2010. Coseismic fault slip of the 2008 Mw7.9 Wenchuan earthquake estimated from InSAR and GPS measurements, *Geophys. Res. Lett.,* **37**(L01302), doi:10.1029/2009GL041213.

Fialko, Y., Simons, M. & Agnew, D., 2001. The complete (3-D) surface displacement field in the epicentral area of the 1999 Mw 7.1 Hector Mine earthquake, California, from space geodetic observations, *Geophys. Res. Lett.,* **28**(16), 3063–3066.

Funning, G.J., Parsons, B., Wright, T.J., Jackson, J.A. & Fielding, E.J., 2005. Surface displacements and source parameters of the 2003 Bam (Iran) earthquake from Envisat advanced synthetic aperture radar imagery, *J. geophys. Res.,* **110**(B09406), doi:10.1029/2004JB003338.

Gudmundsson, S., Sigmundsson, F. & Carstensen, J.M., 2002. Three-Dimensional Surface Motion Maps Estimated from Combined Interferometric Synthetic Aperture Radar and GPS Data, *J. geophys. Res.,* **107**(B10), 2250.

Guglielmino, F., Nunnari, G., Puglisi, G. & Spata, A., 2011. Simultaneous and integrated strain tensor estimation from geodetic and satellite deformation measurements to obtain three-dimensional displacement maps, *IEEE Trans. Geosci. Remote Sens.,* **49**(6), 1815–1826.

Grapenthin, R. & Freymueller, J.T., 2011. The dynamics of a seismic wave field: Animation and analysis of kinematic GPS data recorded during the 2011 Tohoku-oki earthquake, Japan, *Geophys. Res. Lett.,* **38**(L18308), doi:10.1029/2011GL048405.

Hashimoto, C., Noda, A., Sagiya, T. & Matsu'ura, M., 2009. Interplate seismogenic zones along the Kuril-Japan trench inferred from GPS data inversion, *Nat. Geosci.,* **2**(2), 141–144.

Hashimoto, C., Noda, A. & Matsu'ura, M., 2012. The Mw 9.0 northeast Japan earthquake: total rupture of a basement asperity, *Geophys. J. Int.,* **189,** 1–5.

Hu, J., Li, Z.W., Zhu, J.J., Ding, X.L. & Ren, X.C., 2010. Inferring three-dimensional surface displacement field by combining SAR interferometric phase and amplitude information of ascending and descending orbits, *Sci. China Earth Sci.,* **53,** 550–560.

Hu, J., Li, Z.W., Sun, Q., Zhu, J.J. & Ding, X.L., 2012. Three-dimensional surface displacements from InSAR and GPS measurements with variance component estimation, *IEEE Geosci. Remote Sens. Lett.,* **9**(4), 754–758.

Kato, A., Obara, K., Igarashi, T., Tsuruoka, H., Nakagawa, S. & Hirata, N., 2012. Propagation of slow slip leading up to the 2011 Mw 9.0 Tohoku-Oki earthquake, *Science,* **335,** doi:10.1126/science.1215141.

Kobayashi, T., Tobita, M., Nishimura, T., Suzuki, A., Noguchi, Y. & Yamanaka, M., 2011. Crustal deformation map for the 2011 off the Pacific coast of Tohoku Earthquake, detected by InSAR analysis combined with GEONET data, *Earth Planets Space,* **63**(7), 621–625.

Li, Z.W., Ding, X.L., Zheng, D.W. & Huang, C., 2008. Least squares based filter for remote sensing image noise reduction, *IEEE Trans. Geosci. Remote Sens.,* **47**(7), 2044–2049.

Li, Z.W., Xu, W.B., Feng, G.C., Hu, J., Wang, C.C., Ding, X.L. & Zhu, J.J., 2012. Correcting atmospheric effects on InSAR with MERIS water vapour data and elevation-dependent interpolation model, *Geophys. J. Int.,* **189**(2), 898–910.

Liu, H.X., Zhao, Z.Y., Yu, J. & Jezek, K., 2008. Simultaneous least squares adjustment of multiframe velocities derived from interferometric and speckle-tracking methods, *IEEE Geosci. Remote Sens. Lett.,* **5**(2), 289–293.

Ozawa, S., Nishimura, T., Suito, H., Kobayashi, T., Tobital, M. & Imakiire, T., 2011 Coseismic and postseismic slip of the 2011 magnitude-9 Tohoku-Oki earthquake, *Nature,* **475,** doi:10.1038/nature10227.

Sagiya, T., 2004. A decade of GEONET: 1994–2003-The continuous GPS observation in Japan and its impact on earthquake studies, *Earth Planets Space,* **56,** xxix–xli.

Samsonov, S.V., Tiampo, K.F., Rundle, J.B. & Li, Z.H., 2007. Application of DInSAR-GPS Optimization for Derivation of Fine-Scale Surface Motion Maps of Southern California, *IEEE Trans. Geosci. Remote Sens.,* **45**(2), 512–521.

Sato, M., Ishikawa, T., Ujihara, N., Yoshida, S., Fujita, M., Mochizuki, M. & Asada, A., 2011. Displacement above the hypocenter of the 2011 Tohoku-Oki earthquake, *Science,* **332**(6036), 1395.

Shao, Z.G., Wu, Y.Q., Jiang, Z.S. & Zhang, L.P., 2011. The analysis of coseismic slip and near-field deformation about Japanese 9.0 earthquake based on the GPS observation, *Chin. J. Geophys.,* **54**(9), 2243–2249 (in Chinese).

Vanicek, P., Grafarend, E.W. & Berber, M., 2008. Strain invariants, *J. Geod.,* **82,** 263–268.

Wessel, P. & Smith, W.H.F., 1998. New improved version of the Generic Mapping Tools released, *EOS, Trans. Am. geophys. Un.,* **79,** 579, doi:10.1029/98EO00426.

Wright, T.J., Parsons, B.E. & Lu, Z., 2004. Toward mapping surface deformation in three dimensions using InSAR, *Geophys. Res. Lett.,* **31**(1), doi:10.1029/2003gl018827.

Xiong, Z., Tong, Q.X. & Zheng, L.F., 2000. The effects of several smoothness and interpolation algorithm on image spatial resolution evaluation, *J. Remote Sen.,* **4**(1), 36–40 (in Chinese).

SUPPORTING INFORMATION

Additional Supporting Information may be found in the online version of this article:

Figure S1. The azimuth displacement map of the 2011 M_w 9.0 Tohoku-Oki earthquake derived from offset-tracking method.

Figure S2. (a, b) The standard deviation maps of the PALSAR and ASAR LOS measurements, respectively. (c, d) The standard deviation maps of the interpolated GPS measurements in the east–west and north–south directions, respectively. The dashed box shows the location of the two aftershocks occurred in 19 March and 11 April 2011.

Figure S3. The standard deviation maps of the 3-D coseismic surface displacements of the Tohoku-Oki earthquake obtained from InSAR and GPS integration. (a) Vertical, (b) east–west and (c) north–south components (http://gji.oxfordjournals.org/lookup/suppl/doi:10.1093/gji/ggs033/-/DC1).

Please note: Oxford University Press are not responsible for the content or functionality of any supporting materials supplied by the authors. Any queries (other than missing material) should be directed to the corresponding author for the article.

Downloaded from http://gji.oxfordjournals.org/ at The Hong Kong Polytechnic University on February 11, 2015